Available online at website: https://journal.bcrec.id/index.php/bcrec

Bulletin of Chemical Reaction Engineering & Catalysis, 20 (4) 2025, 582-593

Original Research Article

Green Synthesis of Chitosan-Assisted ZnO Nanoparticles and Their Photocatalytic Application in ZnO/TiO_2 Composites for Isopropanol Degradation

Le H. Hoang[1,a], Ho G. Quynh[1,a], Mai H. Nghi[1], Nguyen T. T. Phuong[1], Ngo T. H. Duong[1,2], Nguyen Q. Long[1,2,*]

[1]Faculty of Chemical Engineering, Ho Chi Minh City University of Technology (HCMUT), 268 Ly Thuong Kiet Street, Ho Chi Minh City, Vietnam
[2]Vietnam National University Ho Chi Minh City, Ho Chi Minh City, Vietnam.

Received: 2nd July 2025; Revised: 31th August 2025; Accepted: 5th September 2025
Available online: 8th September 2025; Published regularly: December 2025

Abstract

Nano-sized ZnO particles were successfully synthesized via a green, efficient, and chitosan-assisted method, which is both cost-effective and environmentally friendly. The nanoscale characteristics of the synthesized particles were confirmed through various analytical techniques, including X-ray diffraction (XRD), scanning electron microscopy (SEM), nitrogen adsorption–desorption isotherms, diffuse reflectance spectroscopy (DRS), and Fourier-Transform Infrared Spectroscopy (FTIR). This study primarily investigated the photocatalytic performance of ZnO/TiO_2 composites prepared by a simple mechanical mixing approach for the degradation of isopropanol (IPA) in a continuous-flow system under UVA irradiation at room temperature. A range of experimental conditions, including initial IPA concentrations, gas flow rates, relative humidity levels, and the number of UV lamps, were systematically explored. The mechanically mixed ZnO/TiO_2 nanomaterial exhibited enhanced photocatalytic activity compared to pure ZnO. Notably, while commercial TiO_2 showed reduced IPA removal efficiency under humid conditions, the ZnO/TiO_2 composite maintained superior performance, achieving a removal efficiency of 45% over a 3-hour period at 30% relative humidity with an inlet IPA concentration of about 1200 ppmv, a flow rate of 3 L/h, and illumination by four UV lamps.

Keywords: Nanoparticle; ZnO; ZnO/TiO2; Photocatalysis; IPA

How to Cite: Hoang, L. H., Nghi, M. H., Quynh, H. G., Phuong, N. T. T., Duong, N. T. H., Long, N. Q. (2025). Green Synthesis of Chitosan-Assisted ZnO Nanoparticles and Their Photocatalytic Application in ZnO/TiO_2 Composites for Isopropanol Degradation. *Bulletin of Chemical Reaction Engineering & Catalysis*, 20 (4), 582-593. (doi: 10.9767/bcrec.20431)

Permalink/DOI: https://doi.org/10.9767/bcrec.20431

1. Introduction

The rapid expansion of global industries has driven excessive consumption of fossil fuels, raw materials, and industrial chemicals, resulting in significant emissions of harmful gases, particularly volatile organic compounds (VOCs). Existing VOC control technologies are often insufficiently effective or poorly implemented, worsening air pollution and posing serious risks to public health. Consequently, substantial research has focused on developing advanced VOC mitigation technologies that meet increasingly stringent environmental standards. Strategies to reduce VOC emissions follow two main approaches: source reduction and end-of-pipe treatment. Early efforts prioritized improving processes, equipment, and raw materials to minimize VOC generation, prevent leakage, and limit volatilization.

VOC treatment methods are generally classified into recovery-based (adsorption,

* Corresponding Author.
Email: nqlong@hcmut.edu.vn (N.Q. Long)

[a] Le H. Hoang and Ho G. Quynh contributed equally to this work as first authors.

absorption, condensation, membrane separation) and destruction-based (biofiltration, oxidation) techniques. On the one hand, recovery-based approaches can be effective but often face high operational costs, complex waste management, or energy-intensive requirements [1,2]. On the other hand, among destruction methods, biofiltration offers low-cost and eco-friendly operation but is limited by slow, selective degradation [3]. Besides, catalytic oxidation stands out for its high efficiency, low byproduct formation, and lower operating temperatures [4]. In particular, photocatalytic oxidation has emerged as a highly promising strategy, enabling VOC mineralization into CO_2 and water under ambient conditions with minimal secondary pollution. Its widespread application, however, hinges on the development of robust, cost-effective catalysts with high activity and stability.

Numerous studies have demonstrated that TiO_2 is a highly active semiconductor photocatalyst suitable for the treatment of a wide range of contaminants in both liquid and gaseous phases. The photocatalytic mechanism of TiO_2 can be described by the following reactions and Figure 1 [5,6].

$$TiO_2 + h\nu \rightarrow e^- (TiO_2) + h^+ (TiO_2) \quad (1)$$

$$(O_2)_{aq} + e^-_{CB} \rightarrow O_2^{\bullet -} \xrightarrow{H^+} HO_2^{\bullet} \xrightarrow{e^-, H^+} H_2O_2 \quad (2)$$

$$H_2O_2 + O_2^{\bullet -} \rightarrow OH^- + OH^{\bullet} + O_2 \quad (3)$$

$$H_2O_2 \xrightarrow{h\nu} 2OH^{\bullet} \quad (4)$$

$$O_s^{2-} + H^+ + h^+_{VB} \rightarrow OH^{\bullet} \quad (5)$$

$$OH^{\bullet} + VOCs + O_2 \rightarrow CO_2 + H_2O \quad (6)$$

However, a major drawback of semiconductor photocatalysis is the rapid recombination of photogenerated electron–hole pairs, which significantly limits photocatalytic efficiency. This limitation can be addressed through various enhancement strategies, such as doping the semiconductor with non-metal impurities [7], incorporating transition metals [8], and using composite semiconductors [9]. One effective way to enhance photocatalytic efficiency is by designing well-engineered heterojunction photocatalysts, where the interface between two semiconductors with different band structures promotes charge separation and transfer [10] . In fact, nano-sized semiconductors have been shown to effectively enhance the photocatalytic activity of heterojunction systems, because nanostructured materials offer a significantly higher specific surface area compared to their bulk counterparts. When the size of the nanoparticles approaches the quantum confinement limit, the electrons become confined within extremely small spatial regions, comparable to or smaller than the electron's de Broglie wavelength. This spatial confinement alters the electronic energy levels within the material, resulting in distinct properties compared to those observed in the bulk state. Previously, our research team used TiO_2 and carbon quantum dots (CQDs) to deal with the rapid combination of e^-/h^+. However, CDs/TiO_2 photocatalysts still have certain limitations, including low surface area per unit mass, low affinity for organic compounds, and difficulties with recovery and reuse (the catalysts' tendency to agglomerate and clump together prevents light from reaching the active centers on their surface) [11].

Recently, ZnO nanoparticles (NPs) presents a promising alternative, offering advantages such as low capital and operating costs, mild reaction conditions, and the capability to degrade a wide range of hazardous organic compounds in water into CO_2 and H_2O [12]. ZnO has also been extensively studied due to their outstanding

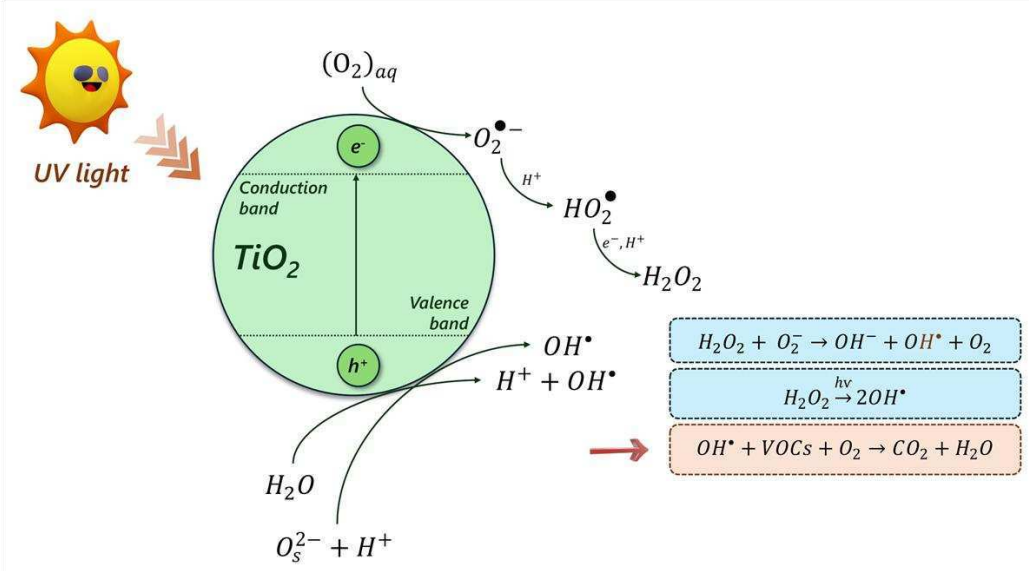

Figure 1. Photocatalytic mechanism for TiO_2.

properties in fields, such as gas sensors [13], optical and electronic devices [14], solar cells [15], drug delivery [16], antibacterial materials [17], and photocatalysis [18]. Furthermore, in recent years, numerous studies have demonstrated the effectiveness of ZnO as a semiconductor component in heterojunction systems for the efficient degradation of various types of pollutants [13,19]. Therefore, this study investigates the photocatalytic efficiency of a heterojunction system constructed using nanosized ZnO particles.

In fact, the similarity in bandgap energies and the alignment of the conduction and valence bands between ZnO and TiO_2 facilitate the efficient transfer of electrons and holes, enabling the formation of effective heterojunctions between the two materials [20-22]. The difference in conduction band positions between ZnO and TiO_2 enables the photogenerated electrons in ZnO to rapidly transfer to TiO_2 upon light absorption. This electron migration promotes efficient charge separation and reduces the recombination rate of electron–hole pairs at the surface. Additionally, the incorporation of ZnO into TiO_2 introduces defects and impurities into the TiO_2 bandgap, which can effectively narrow its bandgap and lower the excitation energy required for the composite material [23].

Unlike most previous studies on ZnO/TiO_2 catalysts, which typically rely on conventional chemical or energy-intensive synthesis routes, this study introduces a green and efficient chitosan-assisted method for producing nanosized ZnO. To the best of our knowledge, this simple and novel approach has not been reported before. The as-synthesized ZnO was mechanically combined with TiO_2 and the composite's photocatalytic performance was tested against isopropanol, a common VOC, to demonstrate its potential for air pollution control.

2. Materials and Methods

2.1 Syntheses and Characterization of Nano ZnO/TiO_2

All chemicals were used without further purification and were purchased from commercial suppliers as follows: zinc(II) chloride ($ZnCl_2$, >98%), acetic acid (>99.5%), and sodium hydroxide (NaOH, >99%) were obtained from Xilong Co., while titanium dioxide (TiO_2) and chitosan were sourced from commercial vendors.

In terms of the catalyst synthesis, initially, 5 g of $ZnCl_2$ was weighed and dispersed in 100 mL of 1% (v/v) acetic acid, followed by sonication in an ultrasonic bath for 15 minutes. Separately, a 1% (w/v) chitosan solution was prepared by dissolving 1 g of chitosan in 1% acetic acid. The two solutions were then combined, adjusted to pH of 5, and stirred at 45 °C for 22 hours. Subsequently, 1 M NaOH was added dropwise to the mixture until the pH reached 10, while maintaining stirring at room temperature. The mixture was aged for an additional 22 hours at room temperature. The resulting solution was filtered and thoroughly washed with distilled water to remove unreacted chitosan and byproducts such as NaCl. The obtained white precipitate was dried at 80 °C for 16 hours. Finally, the dried material was calcined by heating at a rate of 50 °C per 20 minutes up to 550 °C, and then held at this temperature for 3 hours to produce nanosized ZnO.

Next, the mechanical mixing samples were made by physically mixing nano-ZnO and TiO_2 powders in different weight ratios. The mixture was dispersed in 2 mL of pure ethanol (>99.5%) and sonicated for 15 minutes. Subsequently, the samples were heated at 200 °C for 1 hour to evaporate the solvent and remove any adsorbed substances from the surface. Each mixture was applied in successive layers onto the outer surface of a glass tube via the rotary spray-coating technique. During coating, the glass tubes were positioned horizontally and rotated at 140 rpm. The coated catalysts were then heated at 200 °C for 1 hour to activate them prior to the reaction tests. The samples are denoted as M-a:b, where a and b represent the weight fractions of ZnO and TiO_2 in the sample, respectively. Table 1 clearly presents the masses of ZnO and TiO_2 in the different composites.

The structural and physicochemical properties of the prepared catalysts were thoroughly characterized using a combination of analytical techniques. X-ray Powder Diffraction (XRD) analysis was performed using a D2 Phaser instrument (Bruker, Germany) with monochromatic Cu-Kα radiation ($\lambda = 1.5406$ Å), scanning in step-scan mode ($\Delta 2\theta = 0.05°$) over the 2θ range of 10°–80°, to identify crystalline phases and estimate crystallite size. Furthermore, surface area and porosity were determined by nitrogen adsorption–desorption analysis using a NOVA 2200e Quantachrome 10.0 instrument. The Brunauer–Emmett–Teller (BET) method was applied to the adsorption data in the relative pressure range of 0 to 1 to calculate specific surface areas. Moreover, the surface morphology and particle size distribution were examined

Table 1. Mass of ZnO and TiO_2 in composite.

Sample	Weight (g)	
	ZnO	TiO_2
M-1:0	0.2	0
M-1:1	0.1	0.1
M-1:3	0.05	0.15
M-3:1	0.15	0.05
M-0:1	0	0.2

using Scanning Electron Microscopy (SEM) with a JSM-IT200 instrument (JEOL, Japan). In addition, optical properties were investigated using Diffuse Reflectance Spectroscopy (DRS) on a UV-2600 spectrophotometer (Shimadzu, Japan), equipped with an integrating sphere accessory (ISR-2600 Plus). Measurements were conducted in the wavelength range of 220–1400 nm, using halogen and deuterium lamps as light sources and a PMT R928 detector. Besides, Fourier-Transform Infrared Spectroscopy (FTIR) analysis was carried out using an Alpha II instrument (Bruker, Germany) to identify functional groups and surface interactions. Samples were mixed with KBr, pressed into pellets, and analyzed in transmission mode over the spectral range of 4000–500 cm^{-1}.

2.2 Photocatalytic Activity Measurement

The photocatalytic oxidation system was designed to simulate atmospheric conditions suitable for the investigation. Two high-pure gas sources, nitrogen (N_2) and oxygen (O_2) with purities above 99.99%, were mixed at a 4:1 volume ratio to approximate the composition of air. The nitrogen stream was further divided into three separate flows: (1) one stream was passed through a container containing IPA to generate a VOC-laden stream at the desired concentration, (2) another stream was directed through distilled water to introduce water vapor into the system, and (3) a third stream of pure nitrogen was used to dilute the IPA concentration as needed. All gas streams, including oxygen, were precisely controlled using flowmeters and then combined in a mixing vessel to ensure a stable and homogeneous gas mixture before entering the photocatalytic reactor. The mixed gas stream was then passed through the photocatalytic reactor, which was irradiated by four Sanko Denki F10T8BLB lamps with a wavelength of 352 nm and an intensity of 1.5 W. The distance between the UV lamps and the photocatalyst surface was maintained at 2.5 cm. Under standard operating conditions with all four lamps activated, the reaction temperature stabilized at 39 °C, which was maintained by a continuous stream of cooling air provided by a fan positioned at the base of the reactor. The outlet concentration of isopropanol (IPA) during the photocatalytic process was continuously monitored using a Hewlett-Packard 5890 Series II Plus gas chromatograph equipped with a flame ionization detector (FID) and an HP-Plot/Q column (30 m × 0.53 mm). The investigation was carried out to investigate the effect of the ZnO/TiO_2 mixing ratio. the initial VOC concentration, relative humidity, and UV intensity, on the photocatalytic activity of the material.

3. Results and Discussion

3.1. Characterization of the Materials

Regarding the XRD results, Figure 2.a and Figure 2.b illustrate the XRD patterns of M-1:0 and M-0:1, respectively. Sample material M-1:0 is compatible with the ZnO crystalline phase, which has a hexagonal wurtzite structure (JCPDS number 036-1451), because it exhibits characteristic X-ray diffraction peaks at 2θ values of 31.8°, 34.4°, 36.3°, 47.6°, 56.6°, 62.9°, 66.4°, 68.0°, 69.2°, and 77.0°, which correspond to the (100), (002), (101), (102), (110), (103), (200), (112), (201), and (004) planes [24,25]. No additional peaks corresponding to other crystalline phases were observed when compared with the standard diffraction patterns, indicating the purity of the synthesized materials. For the M-0:1 sample, which served as the catalyst, the XRD spectrum exhibited distinct diffraction peaks at 25.5° and 38°, characteristic of the anatase phase of TiO_2, consistent with the JCPDS reference pattern No.

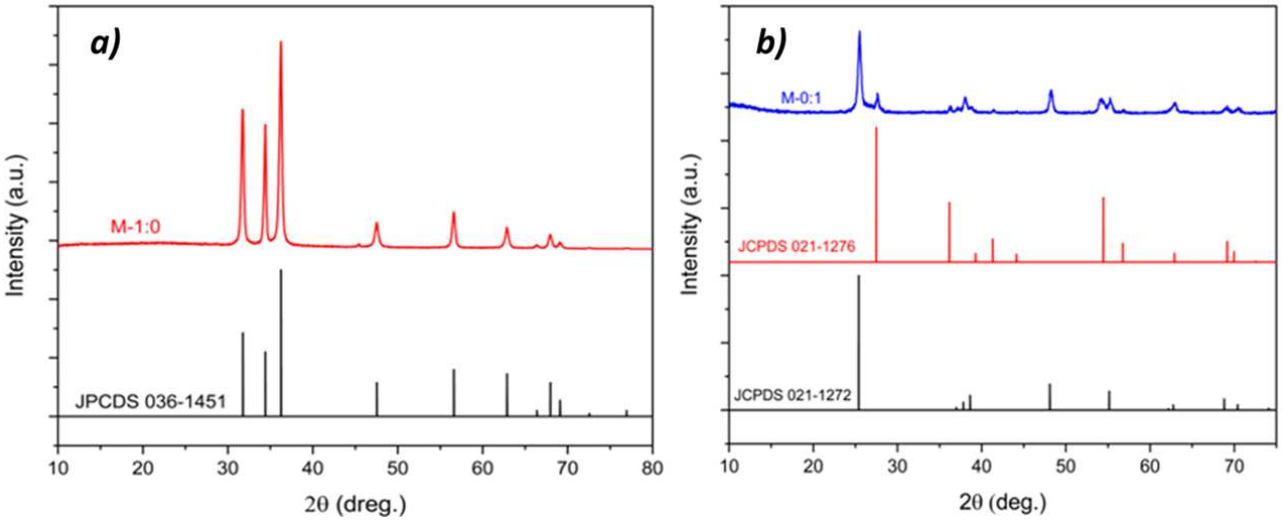

Figure 2. (a) XRD patterns of M-1:0; b) XRD patterns of M-0:1.

021-1272 [26], as well as a peak at 27.6°, corresponding to the rutile phase of TiO_2 (JCPDS No. 029-1360) [27]. From the XRD results of the M-1:0 sample, the average crystal size was determined using the Scherrer equation [28] giving a value of 22 nm. While this method is simple and widely used, it assumes negligible lattice strain and is best suited for relatively simple crystal structures.

For the nitrogen adsorption-desorption analysis, the specific surface area was determined using the BET model. The M-1:0 sample exhibited a BET surface area (S_{BET}) of 16.4 m²/g. Based on the equation: $D = 6000/(d_{BET} \times \rho)$, where the density of ZnO is 5.606 g/cm³, the average particle size was estimated to be approximately 65 nm. The synthesis process for nano-sized ZnO particles was effective in producing the M-1:0 material with a significantly smaller particle size compared to the pristine ZnO sample, which had a particle size of 454 nm and an S_{BET} of 2.4 m²/g [29]. The difference between the average grain size calculated using the BET equation and the values obtained from XRD analysis can be attributed to the tendency of crystals to agglomerate during heat treatment, resulting in larger grain sizes. Table 2 presents the specific surface areas of the three investigated materials. Among them, sample M-0:1 exhibited the highest specific surface area of 49.44 m²/g, approximately three times greater than that of sample M-1:0. This result indicates a superior adsorption capacity of M-0:1, suggesting its ability to accommodate a larger quantity of adsorbates on its surface. In comparison, sample M-1:3 showed a specific surface area of 31.26 m²/g, which is higher than that of M-1:0 but lower than M-0:1. This observation suggests that the mechanical mixing process may induce aggregation and rearrangement of particles, increasing the average particle size and reducing the number of voids and interparticle contact regions. Such rearrangement may also promote the formation of intermetallic phases at specific sites.

In addition, scanning electron microscopy (SEM) was employed to directly examine the morphology and crystallite size of the M-1:0 material. SEM analysis offers localized insights into the surface structure and crystal size. To ensure objectivity, the sample surface was analyzed at two different positions. Figures 3.a and 3.c confirm the uniformity of the material structure, while Figures 3.b and 3.d highlight the crystal sizes observed. The morphology visible in

Table 2. Surface area of the three samples M-a:b.

Sample	BET specific surface area (m²/g)
M-1:0	16.40
M-1:3	31.26
M-0:1	49.44

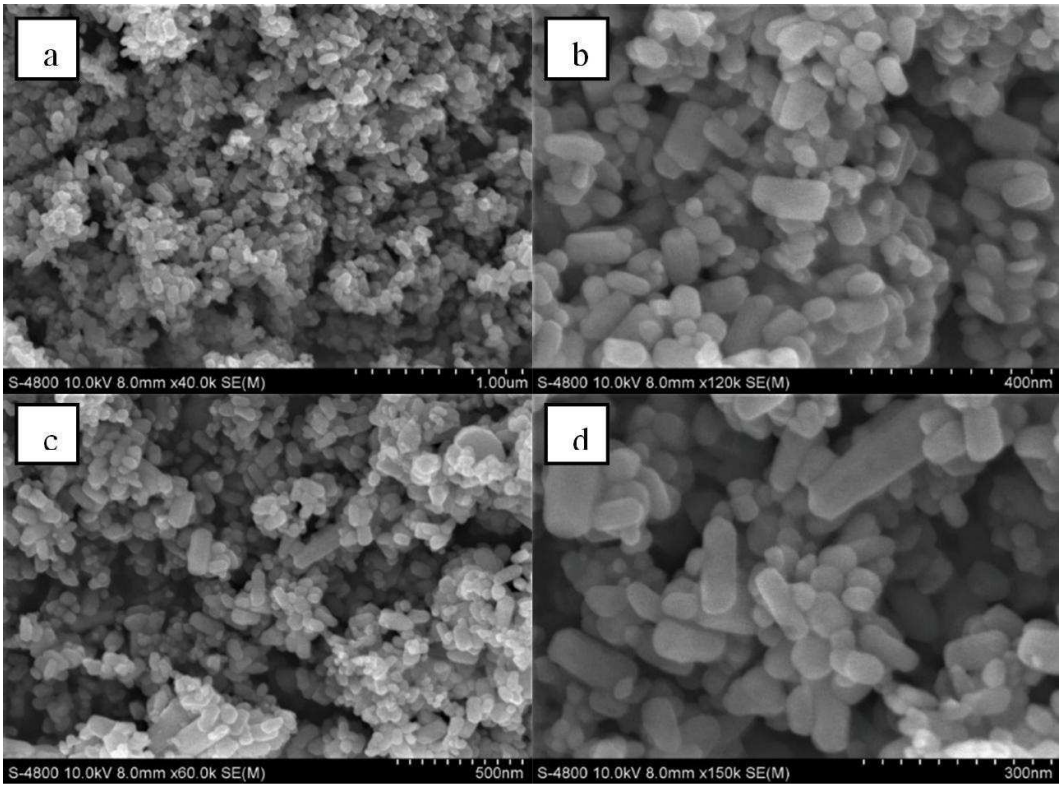

Figure 3. SEM images of sample M-1:0 at different magnifications: (a) ×40.0k, (b) ×120k, (c) ×60.0k, and (d) ×150k

SEM images is consistent with the hexagonal wurtzite structure identified via X-ray diffraction analysis. To further assess the particle size distribution, the SEM images were processed using ImageJ software. As shown in Figure 4, the majority of particles fall within the 30–50 nm range, with an average diameter of 45.25 nm. These findings confirm the successful synthesis of nano-sized ZnO/TiO_2 composite materials.

Furthermore, Fourier-transform infrared (FTIR) spectroscopy was employed to conduct qualitative chemical analysis of sample M-1:0. The FTIR spectrum, presented in Figure 5, shows a distinct absorption peak at 511 cm^{-1}, which corresponds to the stretching vibrations of Zn–O bonds in the ZnO lattice [30]. The absence of additional peaks associated with organic functional groups suggests that no residual organic compounds remained in the sample following the synthesis process.

In addition, diffuse reflectance spectroscopy (DRS) was used to investigate the optical properties of samples M-1:0, M-1:3, and M-0:1, as illustrated in Figure 6.a. The DRS technique provides insights into particle size effects based on the shift in absorption features. For nanomaterials, characteristic absorption edges typically shift toward shorter wavelengths (a blue shift) compared to their bulk counterparts. In this study, the absorption spectrum of sample M-1:0 exhibited a noticeable blue shift, confirming the formation of ZnO nanoparticles. According to Singh et al., the maximum absorption peak of bulk ZnO appears at 374 nm, while ZnO nanoparticles show a peak at 368 nm, indicating a reduction in particle size correlates with a decrease in the absorption wavelength. This observed shift further supports the successful synthesis of nanoscale ZnO in the M-1:0 sample [31]. From Figure 6, the maximum absorption wavelength (λAE of sample M-1:0 is observed in the range of 327–368 nm. For sample M-1:3, the absorption peak lies between 220–320 nm, while for sample M-0:1, it ranges from 220–290 nm. The band gap energy (E_g values of samples M-1:0, M-1:3, and M-0:1, calculated from the Tauc plot in Figure 5.b,

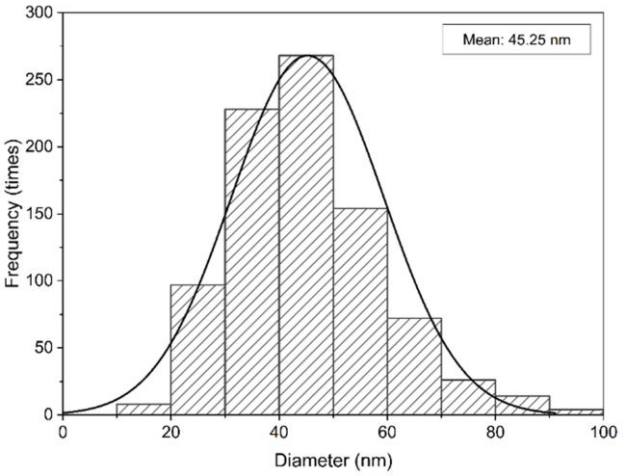

Figure 4. Size distribution graph of sample M-1:0.

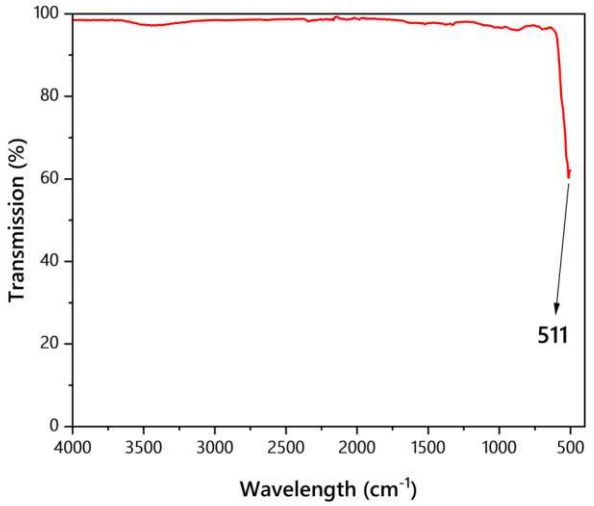

Figure 5. FTIR spectrum of sample M-1:0.sample.

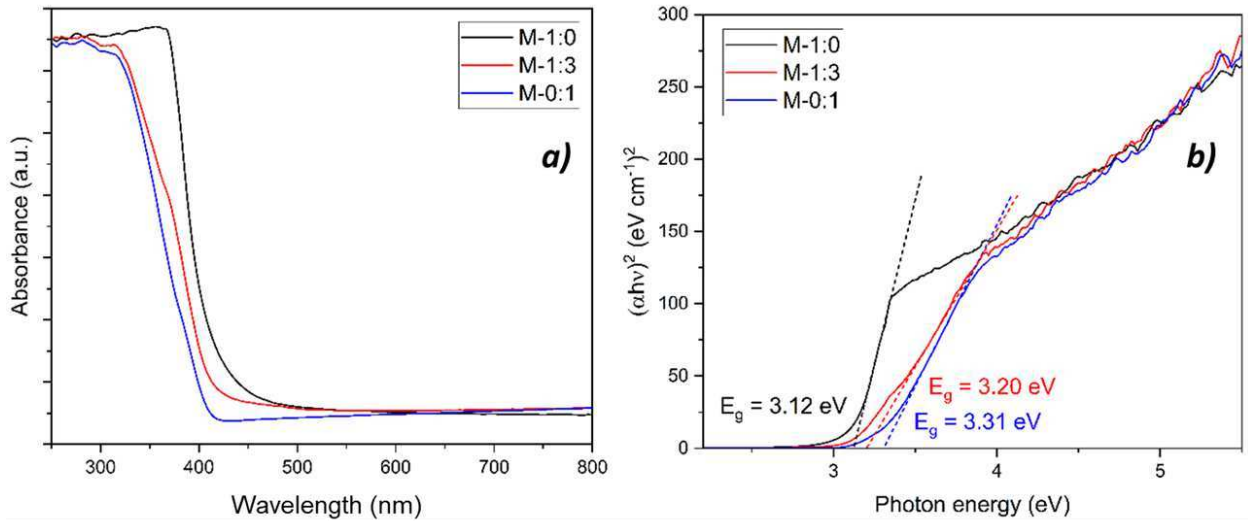

Figure 6 a) DRS spectra of the three samples M-a:b; b) Tauc plot of the three samples M-a:b.

are 3.12 eV, 3.20 eV, and 3.31 eV, respectively. Sample M-1:3 shows improved absorption intensity in the energy range of 200–1400 nm compared to TiO_2. Moreover, its lower band gap value compared to commercial TiO_2 suggests a higher generation of electron-hole pairs under UV light, which enhances its photocatalytic activity. The formed holes can effectively interact with adsorbates on the catalyst surface.

3.2. Effect of ZnO/TiO₂ Ratio on the Catalytic Performance

Figure 7.a illustrates the IPA adsorption capacity of the five samples before participating in the photocatalytic reaction. IPA adsorption on sample M-0:1 occurs rapidly and shows the highest adsorption capacity among all samples, as indicated by the low C/C_0 ratio within the first 15 minutes. This reflects a strong interaction between the catalyst and the gas molecules. In contrast, sample M-1:0 exhibits weaker adsorption, with consistently higher C/C_0 ratios during the same period, suggesting fewer interactions between the catalyst and VOC molecules. This reduced contact lowers the efficiency of the catalytic process and diminishes the material's activity. Furthermore, the surface reactions of adsorbed molecules can alter the chemical properties of the catalyst and reduce its performance. Therefore, optimizing the adsorption step is essential to improve the overall efficiency of the photocatalytic process.

Figure 7.b presents the effect of different mixing ratios on the photocatalytic removal of IPA. The experiments revealed that varying the mixing ratios significantly influenced the photocatalytic performance of the composite materials. Among them, sample M-0:1 demonstrated the highest photocatalytic activity, achieving approximately 91.59% IPA removal after 45 minutes. Sample M-1:3 showed the second-highest efficiency at around 40%, while the remaining samples exhibited removal rates below 20%. These differences in activity can be attributed to the formation of the ZnO/TiO_2 heterojunction and the effect of electron-hole recombination within the semiconductor materials. The dispersion between the two phases is critical in determining photocatalytic performance, and an optimal ZnO/TiO_2 ratio exists for mechanically mixed catalysts to maximize activity. Based on these findings, M-1:3 was selected for further investigation, as it showed the most effective interaction between the two materials among the tested samples.

3.3. Effect of IPA Concentration on the Catalytic Performance of ZnO/TiO₂

Figure 8.a and Figure 8.b illustrate the effects of initial IPA concentration on the adsorption capacity and photocatalytic performance of the M-1:3 sample, respectively. As shown in Figure 8.a, the adsorption capacity is strongly influenced by the initial concentration of IPA. With increasing concentrations, the time required for the material to reach saturation decreases, as more IPA molecules quickly occupy and cover the available surface sites. In Figure 8.b, a clear decline in photocatalytic efficiency is observed with higher IPA concentrations. At an initial concentration of 1174 ppmv, the catalyst achieved approximately 40% removal efficiency within one hour. However, when the initial concentrations increased to 1879 ppmv and 2349 ppmv, the maximum conversion rates dropped to 27.41% and 15.5%, respectively. Although a higher concentration leads to more IPA molecules contacting the catalyst surface, it can also overwhelm the catalyst's capacity [32].

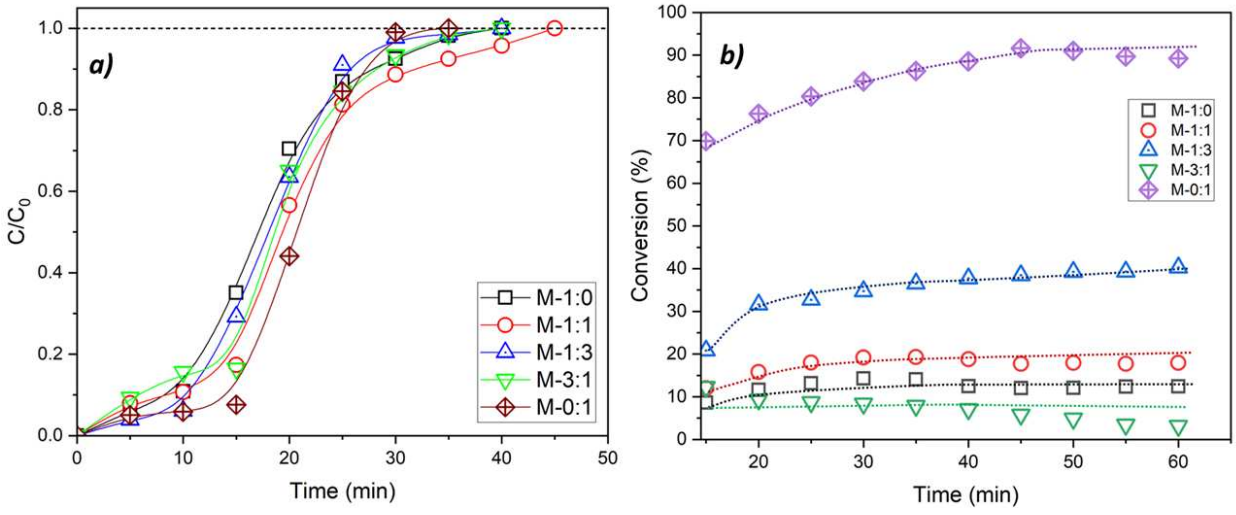

Figure 7 a) IPA adsorption capacity over ZnO/TiO_2 samples with different ratios (CIPA: 1174 ppmv, RH=0%, N_2:O_2 = 8:2, Gas flow rate: 3 L/h); b) IPA removal over ZnO/TiO_2 samples with different ratios (CIPA: 1174 ppmv, RH=0%, N_2:O_2 = 8:2, Gas flow rate: 3 L/h, 4 UV lamps).

This overload may reduce active site availability and lead to the formation of intermediate by-products that inhibit further adsorption and reaction. As a result, the overall efficiency of VOC degradation decreases, and the photocatalytic performance, when normalized by catalyst mass, significantly declines.

3.4. Effect of Humidity on the Catalytic Performance of ZnO/TiO_2

The effects of relative humidity on the IPA adsorption capacity and photocatalytic removal efficiency of the M-1:3 sample are shown in Figure 9.a and Figure 9.b, respectively. Similar to the impact of initial IPA concentration, an increase in humidity leads to a reduction in the time required to reach adsorption saturation. This can be attributed to the competitive adsorption of water vapor on the catalyst surface. Previous studies on humidity's influence in photocatalytic VOC degradation have reported that moderate humidity levels can enhance photocatalytic activity by promoting the formation of hydroxyl (▪OH) radicals on the catalyst surface, which actively participate in VOC degradation [33]. However, when humidity becomes excessive, water molecules begin to dominate the available active sites, hindering the adsorption of IPA. This competitive effect reduces the number of IPA molecules interacting with the catalyst, ultimately lowering its photocatalytic performance.

3.5. Effect of UV Intensity on the Catalytic Performance of ZnO/TiO_2

The effect of UV light intensity on IPA removal efficiency is illustrated in Figure 10.

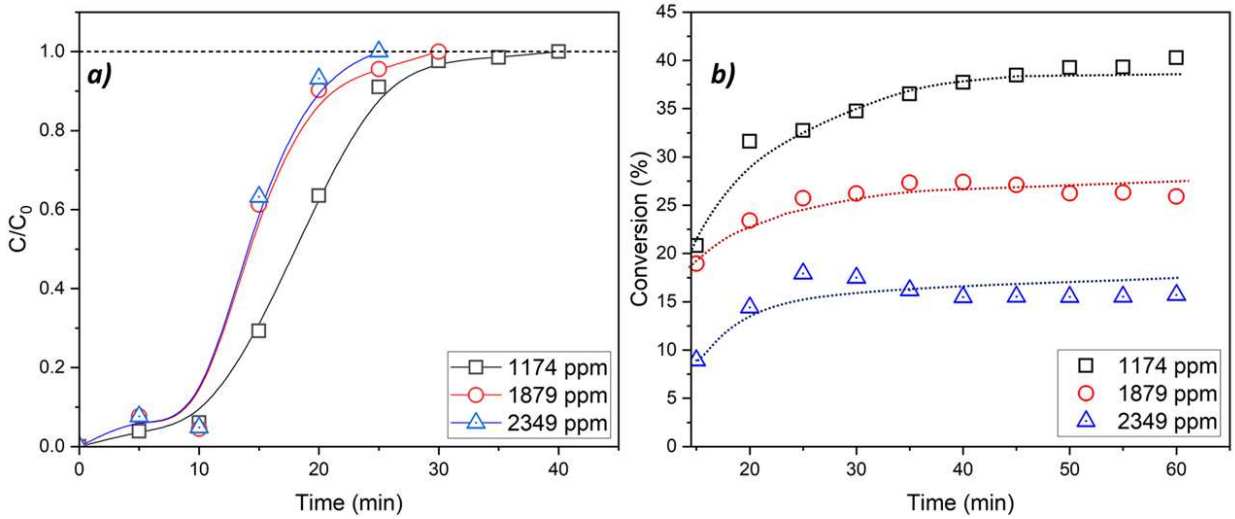

Figure 8. a) Effect of VOC concentration on IPA adsorption capacity of M-1:3 (Gas flow rate: 3 L/h, N_2:O_2 = 8:2, RH=0%); b) Effect of VOC concentration on IPA treatment over M-1:3 (N_2:O_2 = 8:2, RH=0%, Gas flow rate: 3 L/h, 4 UV lamps).

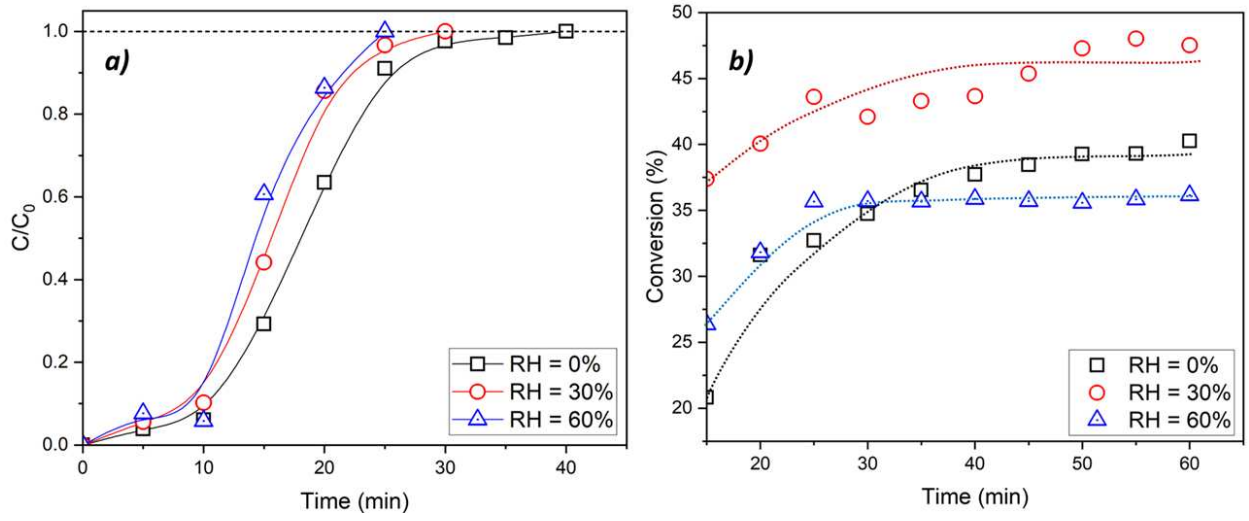

Figure 9. a) Effect of relative humidity on IPA adsorption capacity of M-1:3 (CIPA = 1174 ppmv, N_2:O_2 = 8:2, Gas flow rate: 3 L/h); b) Effect of relative humidity on IPA treatment over M-1:3 (CIPA = 1174 ppmv, N_2:O_2 = 8:2, Gas flow rate: 3 L/h, 4 UV lamps).

Light intensity is a critical parameter influencing the rate of VOC degradation. As shown in the Figure 10, increasing the number of UV lamps from two to four leads to a moderate enhancement in photocatalytic efficiency. Higher UV intensity increases the excitation of electrons (e^-) from the valence band to the conduction band, thereby generating more electron-hole pairs (h^+). These charge carriers are essential for initiating redox reactions involved in VOC degradation. In the presence of H_2O and O_2 in the gas stream, the photocatalyst facilitates their conversion into reactive oxygen species. Specifically, H_2O is oxidized by holes to form hydroxyl radicals (▪OH), while O_2 is reduced by electrons to produce superoxide radicals (▪O_2^-). These highly reactive species play a key role in breaking down VOCs into benign end-products such as CO_2 and H_2O [34]. However, excessive light intensity can induce an overproduction of free radicals that surpass the catalytic capacity of the material. In such cases, the excess radicals may non-selectively oxidize other substances in the gas stream, including non-harmful compounds, thus diminishing the treatment selectivity and potentially causing secondary environmental impacts. Therefore, while increased UV intensity enhances radical formation and improves VOC removal, an optimal light intensity must be determined to balance treatment efficiency and energy consumption, particularly for practical applications.

3.6 Investigation the Photocatalytic Activity Duration over 3 hours

The comparison of photocatalytic activity between M-1:3 and M-0:1 under humid conditions is presented in Figure 11. Under identical reaction conditions, the M-0:1 sample maintains high photocatalytic efficiency and stability, achieving approximately 85% IPA removal after a 3-hour operation period. However, a slight reduction in efficiency is observed for M-0:1 under 30% relative humidity compared to the results under dry conditions (as shown in Figure 6.b), where the efficiency after 60 minutes decreased from 92% to 82%. This decline can be attributed to the increased water vapor content in the gas stream at 30% humidity, which likely exceeds the optimal threshold and leads to competitive adsorption between water molecules and IPA on the catalyst surface, thereby reducing catalytic performance. In contrast, the M-1:3 sample also demonstrates stable activity throughout the reaction period. Notably, under humid conditions, M-1:3 shows a slight improvement in photocatalytic efficiency, increasing from approximately 40% to 45% compared to the dry condition. Despite this improvement, the overall photocatalytic performance of M-1:3 remains lower than that of M-0:1 under the same conditions.

4. Conclusion

In conclusion, the successful synthesis of ZnO nanoparticles on a chitosan substrate via the precipitation method has been achieved. This approach is relatively simple and environmentally friendly compared to conventional synthesis techniques. Characterization by XRD and SEM confirmed that the particle size was within the nanoscale range of 30–50 nm. Diffuse Reflectance Spectroscopy (DRS) further revealed that the ZnO nanoparticles exhibited a maximum absorption wavelength (λAE) between 327–368 nm. Additionally, ZnO/TiO_2 nanocomposites were successfully prepared through mechanical mixing, demonstrating enhanced photocatalytic performance relative to pure ZnO. Among the tested ratios, the ZnO/TiO_2 composite with a 1:3 ratio showed improved photocatalytic activity under humid conditions, maintaining a stable

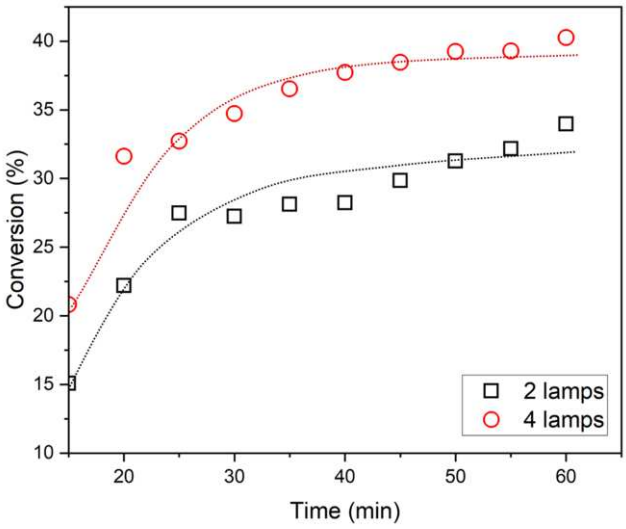

Figure 10. Effect of UV intensity on IPA treatment over M-1:3 (CIPA: 1174 ppmv, N_2:O_2 = 8:2, RH=0%, Gas flow rate: 3 L/h).

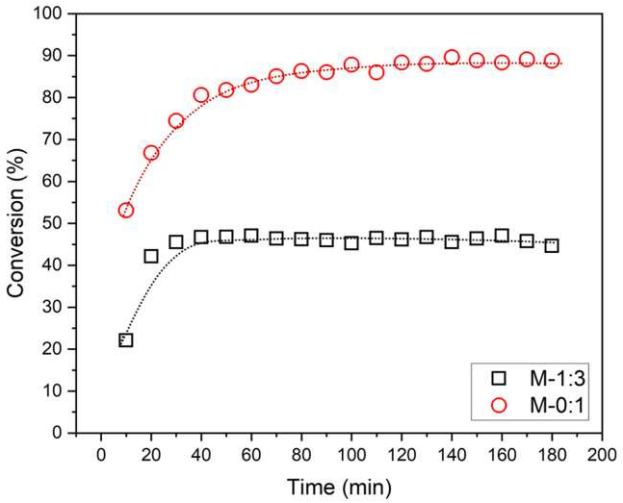

Figure 11. Comparison of IPA removal performance of M-1:3 and M-0:1 samples under humid condition (CIPA: 1174 ppmv, N_2:O_2 = 8:2, RH=30%, Gas flow rate: 3 L/h, 4 UV lamps).

efficiency of approximately 45% over a 3-hour period. However, this performance was still lower than that of pure TiO_2, which achieved up to 88% efficiency under the same conditions. Notably, TiO_2 experienced a decline in activity under humidity compared to dry environments. These findings highlight the importance of further optimizing the mixing ratio to improve photocatalytic efficiency, particularly under high humidity conditions.

Acknowledgments

We acknowledge Ho Chi Minh City University of Technology (HCMUT), VNU-HCM for supporting this study.

Declaration of Generative AI and AI-Assisted Technologies in the Writing Process

During the preparation of this work the authors used ChatGPT by OpenAI in order to assist in language refinement and grammar correction during manuscript preparation. After using this tool, the authors reviewed and edited the content as needed and took full responsibility for the content of the published article.

CRedit Author Statement

Author Contributions: Le H. Hoang: Methodology, Investigation, Formal analysis, Writing – Reviewing and Editing; Mai H. Nghi: Investigation, Formal Analysis, Data Curation; Ho G. Quynh: Writing, Review and Editing; Nguyen T. T. Phuong: Conceptualization, Methodology; Ngo T. H. Duong: Conceptualization, Methodology, Writing - Review & Editing; Nguyen Q. Long: Conceptualization, Methodology, Supervision, Formal analysis, Writing - Review & Editing. All authors have read and agreed to the published version of the manuscript.

References

[1] Li, S., Lin, Y., Liu, G., Shi, C. (2023). Research status of volatile organic compound (VOC) removal technology and prospect of new strategies: a review. *Environmental Science: Processes & Impacts*, 25(4), 727-740. DOI: 10.1039/D2EM00436D.

[2] Belaissaoui, B., Le Moullec, Y., Favre, E. (2016). Energy efficiency of a hybrid membrane/condensation process for VOC (Volatile Organic Compounds) recovery from air: A generic approach. *Energy*, 95, 291-302. DOI: 10.1016/j.energy.2015.12.006.

[3] Espinosa-Ortiz, E.J., R., R.E., Gerlach, R. (2022). Potential use of fungal-bacterial co-cultures for the removal of organic pollutants. *Critical Reviews in Biotechnology*, 42, 3, 361-383. DOI: 10.1080/07388551.2021.1940831.

[4] Minh, N.T., Thanh, L.D., Trung, B.C., An, N.T., Long, N.Q. (2018). Dual functional adsorbent/catalyst of nano-gold/metal oxides supported on carbon grain for low-temperature removal of toluene in the presence of water vapor. *Clean Technologies and Environmental Policy*, 20(8), 1861-1873. DOI: 10.1007/s10098-018-1583-6

[5] Schneider, J., Matsuoka, M., Takeuchi, M., Zhang, J., Horiuchi, Y., Anpo, M., Bahnemann, D.W. (2014). Understanding TiO2 Photocatalysis: Mechanisms and Materials. *Chemical Reviews*, 114, 19, 9919-9986. DOI: 10.1021/cr5001892..

[6] Tu, L.N.Q., Nhan, N.V.H., Van Dung, N., An, N.T., Long, N.Q. (2019). Enhanced photocatalytic performance and moisture tolerance of nano-sized Me/TiO 2–zeolite Y (Me= Au, Pd) for gaseous toluene removal: activity and mechanistic investigation. *Journal of Nanoparticle Research*, 21, 1-19. DOI: 10.1007/s11051-019-4642-y

[7] Nurbayti, S., Adawiah, A., Bale, U.F., Fadhilla, R., Ramadhan, F.N., Zulys, A., Sukandar, D., Saridewi, N., Tulhusna, L. (2024). Sonochemical Assisted Synthesis of Cr-PTC Metal Organic Framework, ZnO, and Fe3O4 Composite and Their Photocatalytic Activity in Methylene Blue Degradation. *Bulletin of Chemical Reaction Engineering & Catalysis*, 19 (2), 318-326. DOI: 10.9767/bcrec.20156.

[8] Twilton, J., Le, C., Zhang, P., Shaw, M.H., Evans, R.W., and MacMillan, D.W.C. (2017). The merger of transition metal and photocatalysis. Nature Reviews Chemistry, 1, no. 7, 0052. Doi: 10.1038/s41570-017-0052.

[9] Nhan, N.V.H., Tu, L.N.Q., Loc, B.T., Vinh, D.C., Phuong, N.T.T., Duong, N.T.H., ... Long, N.Q. (2024). Microwave-assisted synthesis of Carbon Nanodots/TiO2 Composite with enhanced photocatalytic oxidation of VOCs in a continuous Flow reaction. *Topics in Catalysis*, 67(9), 661-669. DOI: 10.1007/s11244-023-01889-2.

[10] Low, J., Yu, J., Jaroniec, M., Wageh, S., Al-Ghamdi, A.A. (2017). Heterojunction photocatalysts. *Advanced Materials*, 29, 20, 1601694. DOI: 10.1002/adma.201601694.

[11] Anh, L.K., Oanh, N.T.K., Hieu, T.L.M., Phuong, N.T.T., Duong, N.T.H., Dung, N.V., Long, N.Q. (2022). Synthesis and Photocatalytic Activity for Toluene Removal of CDs/TiO2 - Zeolite Y. *Bulletin of Chemical Reaction Engineering & Catalysis*, 17 (4), 862-871. DOI: 10.9767/bcrec.17.4.16137.862-871.

[12] Gul, M., Kashif, M., Shahid, K.J.P.R.J. (2024). Eco-friendly approaches in the synthesis of ZnO nanoparticles using plant extract: a review. *Phytopharmacology Research Journal (PRJ),* 3, 2, 1-25.

[13] Kang, Y., Yu, F., Zhang, L., Wang, W., Chen, L., Li, Y. (2021). Review of ZnO-based nanomaterials in gas sensors. *Solid State Ionics*, 360, 115544. DOI: 10.1016/j.ssi.2020.115544.

[14] Sha, R., Basak, A., Maity, P.C., Badhulika, S. (2022). ZnO nano-structured based devices for chemical and optical sensing applications. *Sensors Actuators Reports*, 4, 100098. DOI: 10.1016/j.snr.2022.100098.

[15] Wibowo, A., Marsudi, M.A., Amal, M.I., Ananda, M.B., Stephanie, R., Ardy, H., Diguna, L.J. (2020). ZnO nanostructured materials for emerging solar cell applications. *RSC Advances*, 10, 70, 42838-42859. DOI: 10.1039/D0RA07689A

[16] Huang, X., Zheng, X., Xu, Z., Yi, C. (2017). ZnO-based nanocarriers for drug delivery application: From passive to smart strategies. *International Journal of Pharmaceutics*, 534, 1-2, 190-194. DOI: 10.1016/j.ijpharm.2017.10.008.

[17] Abebe, B., Zereffa, E.A., Tadesse, A., Murthy, H.A. (2020). A review on enhancing the antibacterial activity of ZnO: Mechanisms and microscopic investigation. *Nanoscale Research Letters*, 15, 1-19. DOI: 10.1186/s11671-020-03418-6.

[18] Ong, C.B., Ng, L.Y., Mohammad, A.W. (2018). A review of ZnO nanoparticles as solar photocatalysts: Synthesis, mechanisms and applications. *Renewable Sustainable Energy Reviews*, 81, 536-551. DOI: 10.1016/j.rser.2017.08.020.

[19] Mousa, H.M., Alenezi, J.F., Mohamed, I.M., Yasin, A.S., Hashem, A.-F.M., Abdal-Hay, A. (2021). Synthesis of TiO2@ ZnO heterojunction for dye photodegradation and wastewater treatment. *Journal of Alloys Compounds*, 886, 161169. DOI: 10.1016/j.jallcom.2021.161169.

[20] Wang, J., Wang, G., Wei, X., Liu, G., Li, J. (2018). ZnO nanoparticles implanted in TiO2 macrochannels as an effective direct Z-scheme heterojunction photocatalyst for degradation of RhB. *Applied Surface Science*, 456, 666-675. DOI: 10.1016/j.apsusc.2018.06.182.

[21] Siwińska-Stefańska, K., Kubiak, A., Piasecki, A., Dobrowolska, A., Czaczyk, K., Motylenko, M., Rafaja, D., Ehrlich, H., Jesionowski, T. (2019). Hydrothermal synthesis of multifunctional TiO2-ZnO oxide systems with desired antibacterial and photocatalytic properties. *Applied Surface Science*, 463, 791-801. DOI: 10.1016/j.apsusc.2018.08.256.

[22] Mukhopadhyay, S., Maiti, D., Chatterjee, S., Devi, P.S., Kumar, G.S. (2016). Design and application of Au decorated ZnO/TiO2 as a stable photocatalyst for wide spectral coverage. *Physical Chemistry Chemical Physics*, 18, 46, 31622-31633. DOI: 10.1039/C6CP06903G.

[23] Wang, Y., Zhu, S., Chen, X., Tang, Y., Jiang, Y., Peng, Z., Wang, H. (2014). One-step template-free fabrication of mesoporous ZnO/TiO2 hollow microspheres with enhanced photocatalytic activity. *Applied Surface Science*, 307, 263-271. DOI: 10.1016/j.apsusc.2014.04.023.

[24] Ahmed, N., Majid, A., Khan, M., Rashid, M., Umar, Z., Baig, M. (2018). Synthesis and characterization of Zn/ZnO microspheres on indented sites of silicon substrate. *Mater. Sci.*, 36, 3, 501-508. DOI: 10.2478/msp-2018-0058.

[25] Norouzzadeh, P., Mabhouti, K., Golzan, M., Naderali, R. (2020). Comparative study on dielectric and structural properties of undoped, Mn-doped, and Ni-doped ZnO nanoparticles by impedance spectroscopy analysis. *Journal of Materials Science: Materials in Electronics*, 31, 7335-7347. DOI: 10.1007/s10854-019-02517-0.

[26] Lokesh, B., Rao, N.M. (2016). Effect of Cu-doping on structural, optical and photoluminescence properties of zinc titanates synthesized by solid state reaction. *Journal of Materials Science: Materials in Electronics*, 27, 4253-4258. DOI: 10.1007/s10854-016-4290-2.

[27] Shen, Y., Xu, B., Zhu, S., Zhang, F., Zhao, Q., Li, X. (2018). Enhanced photocatalytic reduction of cadmium on calcium ferrite-based nanocomposites by simulated solar radiation. *Materials Letters*, 211, 142-145. DOI: 10.1016/j.matlet.2017.09.114.

[28] Nath, D., Singh, F., Das, R. (2020). X-ray diffraction analysis by Williamson-Hall, Halder-Wagner and size-strain plot methods of CdSe nanoparticles-a comparative study. *Materials Chemistry Physics*, 239, 122021. DOI: 10.1016/j.matchemphys.2019.122021.

[29] Nguyen, N.T., Nguyen, V.A. (2020). Synthesis, characterization, and photocatalytic activity of ZnO nanomaterials prepared by a green, nonchemical route. *Journal of Nanomaterials* 2020, 1, 1768371. DOI: https://doi.org/10.1155/2020/1768371

[30] Chen, J., Wang, G., Wei, J., Guo, Y. (2019). Effect of sulfur dopant atoms on the electronic band gap and optical properties of tin iodide. *Chemical Physics Letters*, 730, 557-561. DOI: 10.1016/j.cplett.2019.06.056.

[31] Singh, J., Rathi, A., Rawat, M., Kumar, V., Kim, K.-H. (2019). The effect of manganese doping on structural, optical, and photocatalytic activity of zinc oxide nanoparticles. *Composites Part B: Engineering*, 166, 361-370. DOI: 10.1016/j.compositesb.2018.12.006.

[32] da Trindade, L.G., Minervino, G.B., Trench, A.B., Carvalho, M.H., Assis, M., Li, M.S., de Oliveira, A.J., Pereira, E.C., Mazzo, T.M., Longo, E. (2018). Influence of ionic liquid on the photoelectrochemical properties of ZnO particles. *Ceramics International*, 44, 9, 10393-10401. DOI: 10.1016/j.ceramint.2018.03.053.

[33] Nhan, N.V.H., Long, N.Q. (2021). Photodegradation of acetone vapor by carbon dots decorated TiO2 catalyst: effects of experimental conditions. In *Proceedings of the IOP Conference Series: Earth and Environmental Science*, 012014. IOP Publishing.

[34] Shayegan, Z., Lee, C.-S., Haghighat, F. (2018). TiO2 photocatalyst for removal of volatile organic compounds in gas phase–A review. *Chemical Engineering Journal*, 334, 2408-2439. DOI: 10.1016/j.cej.2017.09.153.